Available online at www.sciencedirect.com
SCIENCE DIRECT
Thin Solid Films 469–470 (2004) 388–392
thin solid films
www.elsevier.com/locate/tsf

Cu-penetration induced breakdown mechanism for a-SiCN

C.W. Chen[a], P.T. Liu[b,c,*], T.C. Chang[d,e], J.H. Yang[d], T.M. Tsai[a], H.H. Wu[d], T.Y. Tseng[a]

[a]*Institute of Electronics, National Chiao Tung University, Hsin-Chu, Taiwan*
[b]*Department of Photonics and Display Institute, National Chiao Tung University, Hsin-Chu, Taiwan*
[c]*National Nano Device Laboratories, 1001-1 Ta-Hsueh Rd., Hsin-Chu, Taiwan*
[d]*Department of Physics and Institute of Electro-Optical Engineering, National Sun Yat-Sen University, Kaohsiung, Taiwan*
[e]*Center for Nanoscience and Nanotechnology, National Sun Yat-sen University, Kaohsiung, Taiwan*

Available online 30 October 2004

Abstract

We have investigated the leakage mechanism of amorphous SiCN (a-SiCN) films after bias-temperature-stress (BTS) with Cu electrode. The leakage current became very large and breakdown due to the Cu ions penetration after strict BTS condition. The distribution profile of Cu penetration was depicted by SIMS spectrum. It is apparent that Cu ions penetrated into the a-SiCN film and even reached to the interface between a-SiCN/Si due to BTS. The Cu ions existing in a-SiCN would be taken as trap states and could enhance the carriers to transport. The main characteristics of post-breakdown a-SiCN followed the space-charge-limited current (SCLC) mechanism at 298 K. With decreasing the temperature to 100 K, the Fowler–Nordheim tunneling dominated the conduction in medium fields. However, electrons obeyed the SCLC again in high fields (>3.3 MV/cm) at 100 K. We purpose a physical model to interpret the leakage mechanism of breakdown a-SiCN films due to Cu ions.
© 2004 Elsevier B.V. All rights reserved.

Keywords: Dielectrics; Electrical properties and measurements

1. Introduction

To reduce RC-delay, copper wiring and low-*k* dielectrics are currently used in ultra large-scale integrated (ULSI) circuits [1]. Compared to Al wiring, Cu has better resistance toward electromigration. However, one of the reliability issues in Cu metallization is dielectric degradation caused by Cu ion penetration. Copper could rapidly drift in silica-based low-*k* dielectrics during bias-temperature stressing (BTS) [2]. Therefore, it is necessary to introduce a barrier dielectric between Cu wiring and dielectric insulator to prevent the Cu ion drift/diffusion [3,4]. SiN is generally a barrier dielectric and could efficiently prevent the Cu drift [5]. However, the dielectric constant of SiN is larger (~7). To reduce the effective capacitance of Inter-Metal Dielectrics (IMD) and Inter-Layer Dielectrics (ILD), SiN must be substituted [6]. Implementations of Cu diffusion barrier with dielectric having a *k*-value are more effective in reducing interconnected capacitance. Studies on barrier dielectrics which have lower dielectric constants related to SiN would be attractive [7,8]. Recently, some SiC-based materials with $k<5$ were proposed as barrier dielectrics [9,10].

In this work, we study the amorphous SiCN (a-SiCN) with $k=4.4$ deposited by a plasma-enhanced chemical vapor deposition (PECVD) system. We report the conduction behaviors of post-breakdown (P.B.) a-SiCN film due to Cu penetration. Moreover, a physical model to depict the breakdown mechanism is proposed according to SIMS and electrical characteristics.

2. Experimental details

The amorphous SiCN films were deposited with tri-methyl-silane source using PECVD system. The deposition temperature was 350 °C. The pressure in the chamber is kept at 3 Torr during the deposition. The a-SiCN film was

* Corresponding author. National Nano Device Laboratories, 1001-1 Ta-Hsueh Rd., Hsin-Chu, Taiwan. Tel.: +886 3 5726100x7721; fax: +886 3 172271.
E-mail address: ptliu@ndl.gov.tw (P.T. Liu).

0040-6090/$ - see front matter © 2004 Elsevier B.V. All rights reserved.
doi:10.1016/j.tsf.2004.08.161

deposited on p-type silicon wafer with a resistivity of 15–25 Ω cm. The infrared spectrometry was performed from 4000 to 400 cm^{-1} using a Fourier transform infrared (FTIR) spectrometer calibrated to an unprocessed bare wafer, for determining the chemical structure of the a-SiCN film. The refractive index and thickness of the silicon carbide with or without nitrogen were measured with an n&k analyzer and SORRA ellipsometer. Metal-insulator-semiconductor (MIS) structures of Cu/a-SiCN/silicon were used to investigate the behavior of electrical characteristics.

The dielectric constant and leakage current of the a-SiCN films were investigated using capacitance–voltage (*C–V*) and current–voltage (*I–V*) characteristics measurement on metal-insulator-semiconductor (MIS) capacitor structure. A Keithley Model 82 CV meter at 1 MHz was used to measure the dielectric constant of the film with a gate electrode area of 0.0053 cm^2. The current–voltage (*I–V*) characteristics of a-SiCN films were measured by an HP4156. The gate-electrode area of the MIS structure was 0.00133 cm^2 for *I–V* measurement.

The completed Cu-gated MIS capacitors were then bias-temperature-stressed (BTS) at 150 °C with gate electrode biases (V_{gate}). The stress time was 1000 s, which is long enough for the mobile charges to drift across the stacked insulator layer [11]. The bias was provided by an HP4156 semiconductor parameter analyzer.

3. Results and discussions

Fig. 1 shows FTIR spectrum of a-SiCN film and the important regions of spectrum were labeled in the figure and indicated as follows. The peak at 780 cm^{-1} is identified as Si–C stretching bond. Si–CH_2–Si rock and C–H wag peak are near 990 cm^{-1}, Si–N bond is at 930 cm^{-1}, Si–CH_3 bending peak is at 1245 cm^{-1}, Si–H stretching peak is near 2100 cm^{-1}, and C–H stretching peak is near 2960 cm^{-1}. All of these bonds make the surface of the silicon carbide film hydrophobic [12]. The thickness of a-SiCN in this study is 100 nm determined by n&k analyzer and the dielectric constant is 4.4.

The *J–E* curves of a-SiCN with MIS structure, Cu/a-SiCN/Si, after BTS measurement at 150 °C in the electric field 5.0 MV/cm and the standard (STD) one are demonstrated in Fig. 2, respectively. The leakage currents of stressed a-SiCN sample increased abruptly, indicating breakdown.

We have reported that the conduction behavior of as-deposited a-SiCN is Poole–Frenkel at high electric field (>2.5 MV/cm). Poole–Frenkel (P–F) [13,14] emission is due to field-enhanced thermal excitation of trapped electrons in the insulator into the conduction band. The current density is given by:

$$J = J_0 \exp\left(\frac{\beta_{PF} E^{1/2} - \phi_{PF}}{k_B T}\right) \quad (1)$$

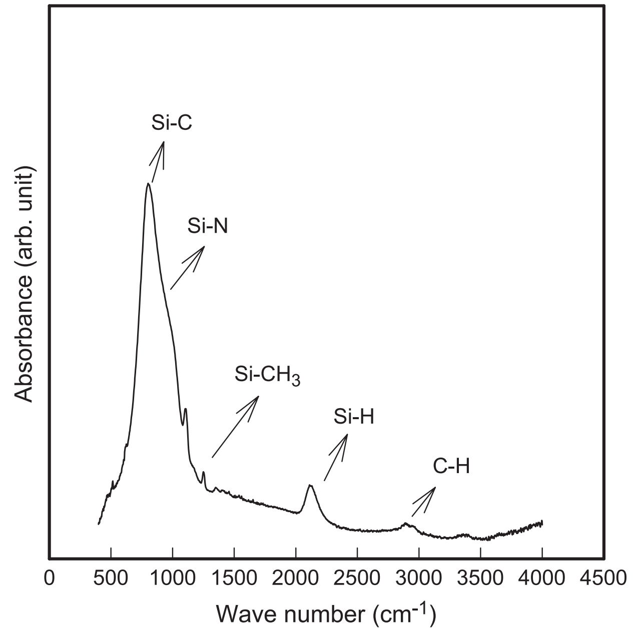

Fig. 1. FTIR spectrum of a-SiCN film and the important regions of film were labeled as Si–C (780 cm^{-1}), Si–N (930 cm^{-1}), Si–CH_2 (990 cm^{-1}), Si–CH_3 (1245 cm^{-1}), Si–H 2100 (cm^{-1}), and C–H (2960 cm^{-1}).

where $\beta_{PF}=(e^3/\pi\varepsilon_0\varepsilon)^{1/2}$, A^* effective Richardson constant, ϕ_{PF} the contact potential barrier, k_B the Boltzmann constant, e the electronic charge, E the applied electric field, ε_0 the dielectric constant of free space, and ε the relative dielectric constant. Poole–Frenkel mechanism can be identified by comparing the theoretical value of β_{PF} with the experimental value of β_{exp} obtained by calculating the slope of the curve ln $(J/E)-E^{1/2}$. Fig. 3 shows that the logarithm of leakage current of a-SiCN sample is linearly related to the square root of the applied electric field, which is close to Poole–Frenkel emission. The value of $\beta_{exp}=5.8\times10^{-23}$ (J $m^{1/2}/V^{1/2}$) which is close to the theoretical value of $\beta_{PF}=5.72\times10^{-23}$ (J $m^{1/2}/V^{1/2}$) as the dielectric constant is 4.4.

Fig. 4 illustrated the SIMS spectrum of post-breakdown a-SiCN film after BTS. It is clear that the copper counts in the post-breakdown a-SiCN films of the MIS structure. However, the Cu peak was un-detected in as-deposited film. The distribution profile of Cu in post-breakdown a-SiCN films was numerous near Cu electrode and reduced at silicon interface. In order to investigate the breakdown characteristics, the conduction behavior of the post-breakdown a-SiCN films were measured for temperature between 50 and 298 K.

The temperature dependence of post-breakdown a-SiCN film was displayed in Fig. 2. The current density of post-breakdown sample was measured at 298 K (curve I), 100K (curve II), and 50 K (curve III), respectively. The current of breakdown sample is obviously decreased with decreasing the temperature from 298 to 100 K. But the conduction characteristics of 100 and 50 K are similar. In addition, note that there are two distinct regions in curve II (100 K) and III (50 K). At medium fields, the current varies exponentially

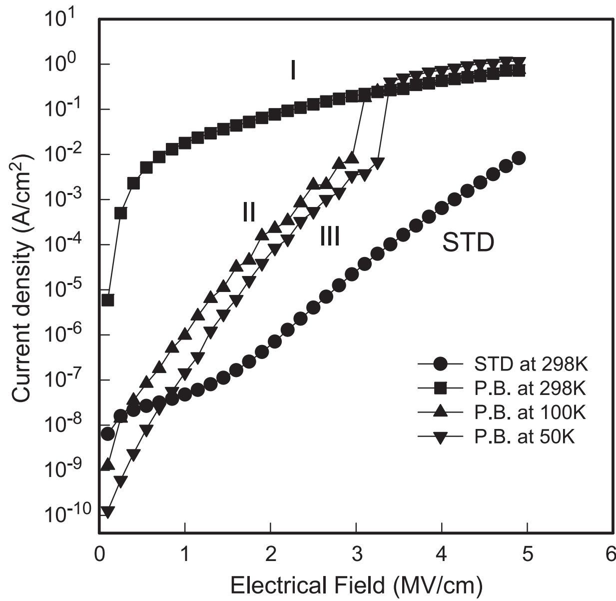

Fig. 2. This shows the *J–E* curves of a-SiCN (STD, as-deposited sample measured at 298 K; curve I, post-breakdown (P.B.) sample measured at 298 K; curve II, P.B. sample measured at 100 K; curve III, P.B. sample measured at 50 K).

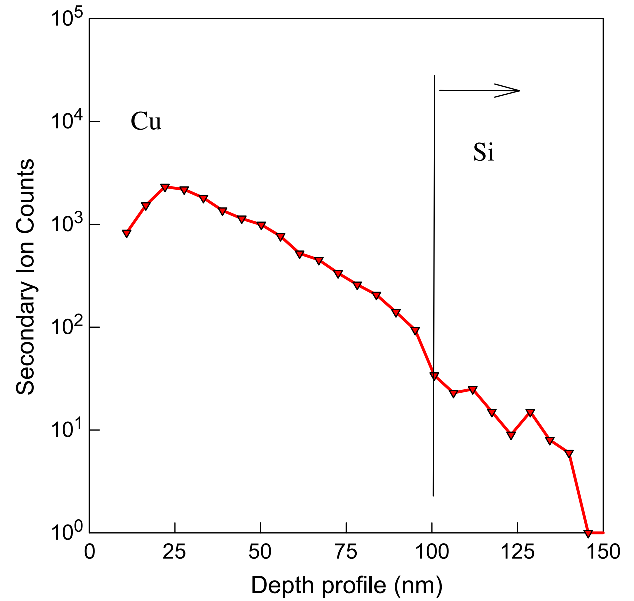

Fig. 4. The SIMS spectrum of post-breakdown SiCN film during BTS measurement. It is observed that Cu ions penetrated through the a-SiCN films.

with the field; in high electric fields (>3.3 MV/cm) the characteristic deviates from the exponential dependence.

To realize the current behaviors of post-breakdown film, electrical characteristics are analyzed with typical conduction processes in insulator such as Poole–Frenkel emission, Schottky emission [13], space-charge-limited current [15,16], and Fowler–Nordheim tunneling [17,18]. We find that the leakage current of post-breakdown a-SiCN at 298 K, curve I, is linearly related to square of the applied electric field, which corresponds to space-charge-limited current (SCLC) mechanism. As considering the SCLC conduction, the current density J can be expressed as the following equation,

$$J = \frac{9\varepsilon_0 \varepsilon \mu \theta V^2}{8d^3} \propto E^2 \quad (2)$$

where μ is the free carrier mobility, ε_0 the permittivity of free space, ε the relative dielectric constant of the sample material, d the sample thickness, and θ is the ratio of the free charge carriers to trapped ones, which takes into account the trapping centers (impurity centers) concentration and their distribution. The SCLC curves are usually interpreted in terms of charge injection and subsequent filling of the impurity/trapping centers giving rise to the progressively square type dependence of the *J–E* characteristics. Fig. 5, transformed from curve I, shows that J is linearly proportional to E^2 at high electric field. Notably, conduction behaviors at low temperature, 100 and 50 K, also obey the SCLC at high fields (>3.3 MV/cm) in curves I and II.

On the other hand, the electrical characteristics of post-breakdown a-SiCN at low temperature, curve II and curve III, follow the Fowler–Nordheim (FN) conduction in medium fields, see Fig. 6. It is generally accepted that the tunneling current through a insulator layer can be represented by the Fowler–Nordheim (FN) expression [17,18]

$$J = K_1 E^2 \exp(K_2/E) \quad (3)$$

where J is the current density, E is the electric field at the insulator, and K_1 and K_2 are two constants dependent on the cathode barrier height, and the electron effective mass. Eq. (3) applies to triangular potential barriers pertinent to MIS structures when qV_g is greater than barrier height, where q is the electron charge, V_g is the gate voltage.

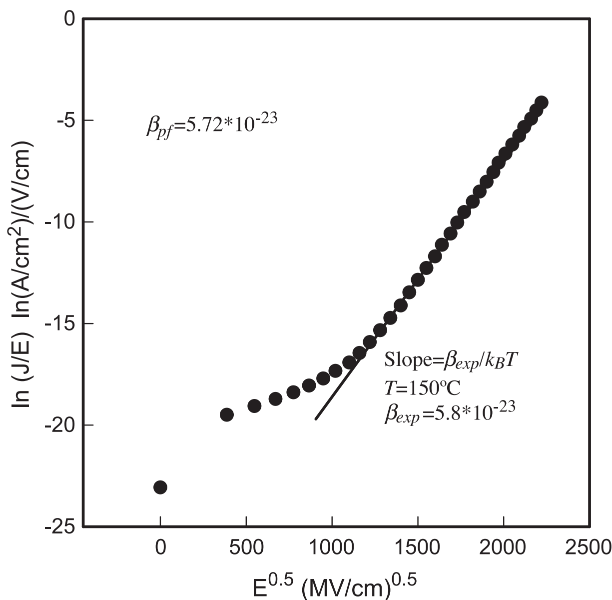

Fig. 3. *J–E* curve on a log (*J/E*) versus $E^{1/2}$ plot of as-deposited a-SiCN film showing Poole–Fenkel conduction at high electric field region.

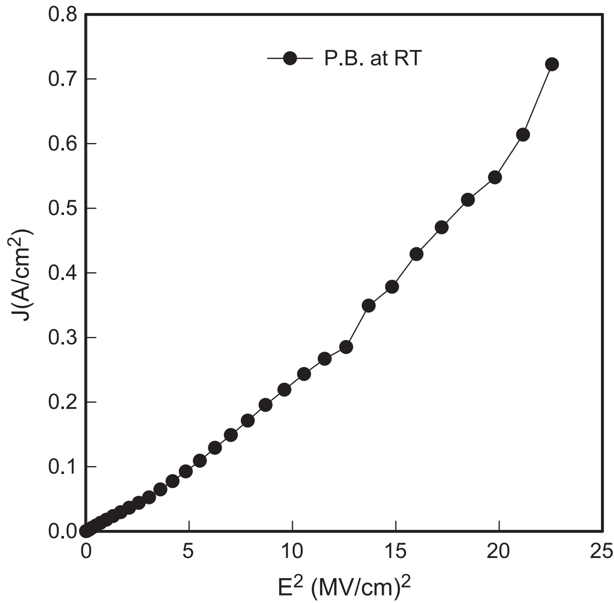

Fig. 5. J–E^2 characteristic of post-breakdown a-SiCN measured at room temperature.

Based on the observation described herein, we proposed a model to depict the conduction characteristics of breakdown a-SiCN caused by Cu penetration. The Cu ions would ionize from Cu electrode and drift in high electrical field at high temperature during BTS [11]. The Cu ions are regarded as trap centers in dielectrics which could assist the carrier to transport [19,20]. The large amount of traps would induce band-gap narrowing in insulator [21]. When the number of traps reaches a critical amount, a conduction filament region [22] which loses its dielectric property is formed and composed of numerous Cu impurity/traps. According to SIMS spectrum, the number of Cu near silicon interface was reduced and assuming an energetic barrier inside the a-SiCN film, a cross-sectional view in real space of post-breakdown is given in Fig. 7(a). In Fig. 7(a), the a-SiCN films are divided into two regions, a conduction filament region (labeled A) [22] and a barrier (labeled B). The real space structure is transformed into energy band-diagram scheme for electrons drawn in Fig. 7(b). Since region A is a conduction filament region, the conduction band is connected smoothly to Fermi-level of Cu electrode. With reducing Cu impurity/traps toward silicon interface, the band-gap is gradually arising and the dielectric property is getting similar to un-degraded sample. However, the band-gap narrowing would appear at a-SiCN/Si interface since the Cu ions penetrated through the film. As a result, the schematic drawing of energy band diagram of breakdown a-SiCN was depicted in Fig. 7(b). It is worthy to mention that greater part of applied voltage should be dropped at barrier region because it plays as the large resistance at low temperature. The effective fields applied on the barrier region must be higher than that we displayed in curves II and III. Consequently, the requirement of F–N tunneling, which should occur at high electrical field, is achieved. The conduction current in post-breakdown SiCN films can be separated into two components: J1 and J2. The J1 is the thermal emission of trap electrons in insulator. The current J2 is due to tunnel emission of trapped electrons into the conduction band of silicon.

The electrons can easily transport from metal electrode to post-breakdown a-SiCN due to the continuation of conduction band between metal and a-SiCN. In addition, electrons have enough energy to jump across the barrier height between a-SiCN and silicon at 298 K. Some transporting electrons are trapped at spatial traps caused by Cu penetration. The dominant characteristic is the SCLC

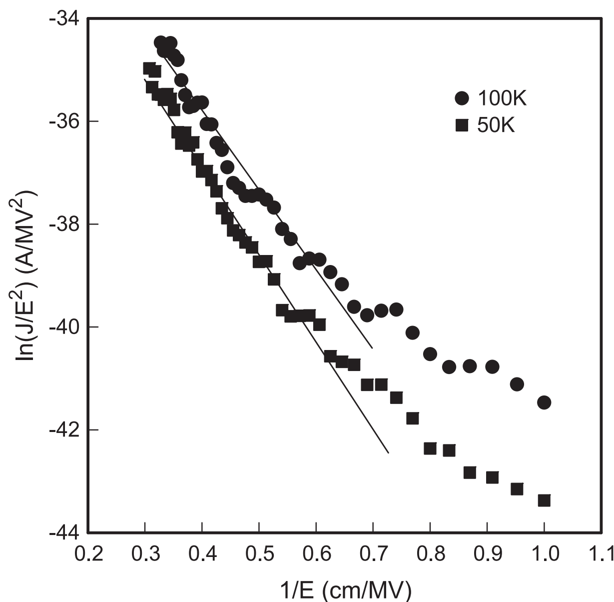

Fig. 6. The conduction characteristics of post-breakdown a-SiCN at low temperature. ln(J/E^2)$-1/E$ showing the Fowler–Nordheim (FN) conduction.

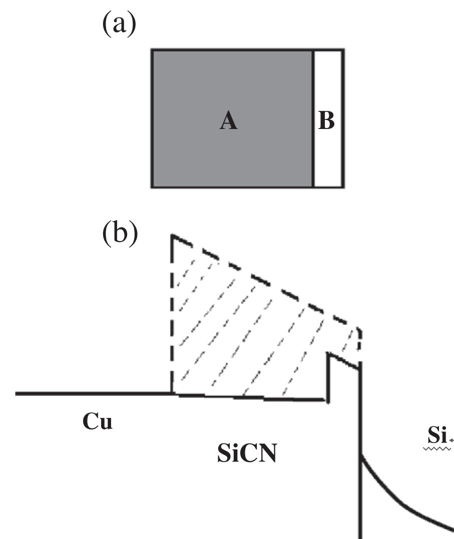

Fig. 7. (a) A cross-sectional view in real space of post-breakdown a-SiCN. The post-breakdown sample is composed of two region, conduction filament (labeled A) and barrier (labeled B). (b) energy band-diagram scheme for electrons. At low temperature, electrons conduct by F–N tunneling.

mechanism. With the decrease in temperature, the cooling electrons cannot excite across the barrier with loss thermal energy. Then the dominant characteristic is the F–N tunneling in post-breakdown a-SiCN at low temperature. As larger voltage is applied to the trapezoid potential barrier pertinent, the thinner barrier region is needed for the electrons to tunnel through. Under this situation, the main controller of conduction is trap filling in bulk and SCLC conduction is dominated. This can explain the reason why the F–N conduction turns into SCLC at high fields at low temperature.

4. Conclusions

The electrical characteristics of post-breakdown a-SiCN caused by Cu penetration are investigated. SIMS spectrum shows that Cu ions can penetrate through the film at 150 °C in high fields (5 MV/cm). It is observed that the main conduction of post-breakdown a-SiCN at room temperature (298 K) is space-charge-limited current (SCLC) due to numerous Cu impurity/traps. Moreover, the characteristics at low temperature can be separated into two distinct stages, Fowler–Nordheim tunneling and SCLC conduction. We propose a physical model which post-breakdown a-SiCN was composed of two different conduction regions. It can well describe the electrical variation that resulted from the Cu traps and temperature.

Acknowledgment

This work was performed at National Nano Device Laboratory and was supported by National Nano Device Laboratory under Contract No. 92A0500001 and the National Science Council of the Republic of China under Contract Nos. NSC92-2112-M-110-020 and NSC92-2215-E-110-006.

References

[1] T. Sakurai, IEEE Trans. Electron Devices 40 (1993) 118.
[2] A. Mallikarjunan, S.P. Murarka, T.M. Lu, Appl. Phys. Lett. 79 (2001) 1855.
[3] M. Vogt, M. Kachel, K. Drescher, Mater. Adv. Metallization (1997) 51.
[4] S.G. Lee, Y.J. Kim, S.P. Lee, H.S. Oh, S.J. Lee, M. Kim, I.G. Kim, J.H. Kim, H.J. Shin, J.G. Hong, H.D. Lee, H.K. Kang, Jpn. J. Appl. Phys., Part. 1 40 (4B) (2001) 2663.
[5] M. Tanaka, S. Saida, T. Lijima, Y. Tsunashima, Dig. Tech. Pap.-Symp. VLSI Technol. (1999) 47.
[6] M. Tada, Y. Harada, K. Hijioka, H. Ohtake, T. Takeuchi, S. Saito, T. Onodera, M. Hiroi, N. Furutake, Y. Hayashi, Proc. 2002 IEEE IITC, 2002, p. 12.
[7] M. Foyolle, J. Torres, G. Passemard, F. Fusalba, G. Fanget, D. Louis, L. Arnaud, V. Girault, J. Cluzel, H. Feldis, M. Rivoire, O. Louveau, T. Mourier, L. Broussous, Proc. 2002 IEEE IITC, 2002, p. 39.
[8] Z.C. Wu, Y.C. Lu, C.C. Chiang, M.C. Chen, B.T. Chen, G.J. Wang, Y.T. Chen, J.L. Huang, S.M. Jang, M.S. Liang, Proc. 2002 IEEE IEDM, 2002, p. 595.
[9] B.Y. Tsui, K.L. Fang, S.D. Lee, IEEE Trans. Electron Devices 48 (2001) 2375.
[10] C.C. Chiang, M.C. Chen, Z.C. Wu, L.J. Li, S.M. Jang, C.H. Yu, M.S. Liang, Proc. 2002 IEEE IITC, 2002, p. 200.
[11] A.L.S. Loke, J.T. Wetzel, P.H. Townsend, T. Tanabe, R.N. Vrtis, M.P. Zussman, D. Kumar, C. Ryu, S.S. Wong, IEEE Trans. Electron Devices 11 (1999) 2178.
[12] P.T. Liu, T.C. Chang, Y.S. Mor, S.M. Sze, C.Y. Chang, Jpn. J. Appl. Phys, Part 1 38 (6A) (1999) 3482.
[13] S.M. Sze, Physics of Semiconductor Devices, Wiley, New York, 1981, p. 403, Ch. 7.
[14] W.R. Harrell, J. Frey, Thin Solid Films 352 (1999) 195.
[15] T. Iqbal, C.A. Hogarth, Int. J. Electron. 61 (1986) 555.
[16] T. Iqbal, C.A. Hogarth, Int. J. Electron. 65 (1988) 953.
[17] R. Fowler, L. Nordheim, Proc. R. Soc. London, Ser. A 119 (1928) 173.
[18] G. Pananakakis, G. Ghibaudo, R. Kies, J. Appl. Phys. 78 (1995) 2635.
[19] P.T. Liu, T.C. Chang, Y.L. Yang, Y.F. Chen, S.M. Sze, IEEE Trans. Electron Devices 47 (2000) 1733.
[20] P.T. Liu, T.C. Chang, S.T. Yan, C.H. Li, S.M. Sze, J. Electrochem. Soc. 50 (2) (2003) F7.
[21] W.Y. Loh, B.J. Cho, M.F. Li, J. Appl. Phys. 91 (8) (2002) 5302.
[22] Y. Omura, K. Komiya, J. Appl. Phys. 91 (7) (2002) 4296.